

Synergistic cooling effects (SCEs) of urban green-blue spaces on local thermal environment

A case study in Chongqing, China

Shi, Dachuan; Song, Jiyun; Huang, Jinxin; Zhuang, Chaoqun; Guo, Rui; Gao, Yafeng

Published in:
Sustainable Cities and Society

DOI (link to publication from Publisher):
[10.1016/j.scs.2020.102065](https://doi.org/10.1016/j.scs.2020.102065)

Creative Commons License
CC BY-NC-ND 4.0

Publication date:
2020

Document Version
Accepted author manuscript, peer reviewed version

[Link to publication from Aalborg University](#)

Citation for published version (APA):

Shi, D., Song, J., Huang, J., Zhuang, C., Guo, R., & Gao, Y. (2020). Synergistic cooling effects (SCEs) of urban green-blue spaces on local thermal environment: A case study in Chongqing, China. *Sustainable Cities and Society*, 55(April), Article 102065. <https://doi.org/10.1016/j.scs.2020.102065>

General rights

Copyright and moral rights for the publications made accessible in the public portal are retained by the authors and/or other copyright owners and it is a condition of accessing publications that users recognise and abide by the legal requirements associated with these rights.

- Users may download and print one copy of any publication from the public portal for the purpose of private study or research.
- You may not further distribute the material or use it for any profit-making activity or commercial gain
- You may freely distribute the URL identifying the publication in the public portal -

Take down policy

If you believe that this document breaches copyright please contact us at vbn@aub.aau.dk providing details, and we will remove access to the work immediately and investigate your claim.

Synergistic Cooling Effect (SCE) of Urban Green-blue Spaces on Local Thermal Environment in Hot-humid Climate

Dachuan Shi^a, Jiyun Song^b, Jinxin Huang^a, Chaoqun Zhuang^c, Rui Guo^d, Yafeng Gao^{a*}

^a Joint International Research Laboratory of Green Building and Built Environment, Ministry of Education, Chongqing University, 400044, Chongqing, PR China

^b Department of Mechanical Engineering, the University of Hong Kong, Hong Kong SAR, China

^c Department of Building Services Engineering, the Hong Kong Polytechnic University, Kowloon, Hong Kong, PR China

^d Department of Civil Engineering, Aalborg University, 9220, Aalborg, Denmark

* Corresponding author

Email Address: gaoyafeng79@126.com

Tel: +86 02365128079

Synergistic Cooling Effects (SCEs) of Urban Green-Blue Spaces on Local Thermal Environment: A Case Study in Chongqing, China

ABSTRACT

Both green and blue space are found to be effective for urban heat mitigation and air quality improvement. However, studies on the Synergistic Cooling Effects (SCEs) of green-blue spaces are limited. This paper aims to investigate the SCEs of green-blue spaces in Chongqing, a typical hot humid city in China, through the field measurement and numerical simulation. First, air temperature and relative humidity over different land-use sites (forest, lawn, and impervious pavement) were measured with and without water simultaneously, from July to August, 2018. Experimental results revealed the SCEs of green-blue spaces were obvious in 7–12 m surrounding waterfront areas, where the mean air temperature reduction was 3.3°C higher than the sums of cooling effect of standalone water and forest. Additionally, an ENVI-met model was validated against the measured data before conducting simulation for the study area in five scenarios, including one control group with no trees and four greening cases with different Leaf Area Index (LAI) values to investigate the importance of green infrastructure on the waterfront thermal environment. Simulation results showed that a decrease of 1.0 LAI can lead to a reduction of average air temperature by 0.19–0.31°C, possibly owing to the enhanced ventilation flow.

Keywords: Synergistic Cooling Effects (SCEs); Urban Cool Island (UCI); Thermal environment; Green space; Blue space.

Nomenclatures

<i>SCE</i>	Synergistic cooling effect	<i>LAD</i>	Leaf area density (m^2/m^3)
<i>UGI</i>	Urban green infrastructure	<i>LAI</i>	Leaf area index
<i>UBS</i>	Urban blue space	<i>L_m</i>	Maximal LAD
<i>UCI</i>	Urban cool island	<i>Z_m</i>	Height of the maximal LAD (m)
<i>UHI</i>	Urban heat island	<i>LBC</i>	Lateral boundary conditions
<i>CFD</i>	Computational fluid dynamic	<i>MCII</i>	Mean cool island intensity ($^{\circ}\text{C}$)
<i>LST</i>	Local standard temperature ($^{\circ}\text{C}$)	<i>RMSE</i>	Root means square error
<i>T_a</i>	Air temperature ($^{\circ}\text{C}$)	<i>MAPE</i>	Mean absolute percentage error (%)
<i>T₀</i>	<i>T_a</i> derived from the nearby weather station located in an open space ($^{\circ}\text{C}$)	<i>T_{Mi}</i>	Average <i>T_a</i> of five waterfront sites at each time ($^{\circ}\text{C}$)
<i>RH</i>	Air relative humidity (%)	<i>N</i>	Total of verified sites
<i>T_{a, observed}</i>	Measured air temperature ($^{\circ}\text{C}$)	<i>T_{a, observed}</i>	Measured air relative humidity (%)
Subscript Symbols			
<i>a</i>	Air	<i>m</i>	Maximum
<i>M</i>	Average	<i>i</i>	Number of site
<i>observed</i>	Measured data	<i>predicted</i>	Simulated data

1 Introduction

Continuous urbanization has led to urban ecological landscapes gradually undergoing increasing spatial differentiation, contributing to intensified global warming and the creation of urban heat islands (UHIs) [1][2]. Elevated concentrations of air pollution and extreme heat events resulting from these phenomena lead to increases in peak-hour power-demands and other ecologically adverse outcomes, as well as increases in heat-related morbidity and mortality of urban residents [3][4]. The growing evidence that global warming is occurring and the desire to reduce pollution have driven societies to take stringent action and reshaped public awareness and behavior [5]. In this context, mitigation of both air pollution and the UHI effect is of high societal value, and is thus an area of focus for governments. In response to recent changes in urban microclimates and outdoor thermal comfort, a variety of measures and practices have been proposed or developed – many of them nature-based – to improve thermal comfort and reduce the UHI effect [6].

Urban green infrastructure (UGI) and urban blue space (UBS) are nature-based elements of urban land use that play indispensable roles in improving the urban thermal environment

[7][8][9][10]. UGI provides surface heat-exchange structures that can be regulated to create urban cool islands (UCIs) through shadowing, photosynthesis, evapotranspiration, and air-movement shielding [11][12][13], while UBS lowers air temperature by its large specific heat capacity and radiative characteristics (transmission, absorption, reflection, and atmospheric reverse radiation across the long-wavelength part of the radiation spectrum). UBS enables water surface energy to be transferred through conduction, convection, and advection with water bodies, and thus has a similar cooling effect as UGI in hot weather, alleviating the extreme heat in urban areas [14][15][16][17]. The cooling effect of UGI is influenced by structure, size, shape, vegetation types, and spatial distribution [18], while that of UBS is affected by wind direction, speed, size, urban geometry, and neighborhood building layout [19].

The UCI-generating potential of UGI and UBS has attracted increasing research attention and intensive discussion, with experiments focusing on the quantitative intensity of the UCI effect. In Nagoya, UGI and UBS induced an air temperature reduction of 1.9°C during the summer, and the cooling effect extended 300 m from the green space [20]. Wang and Akbari [21] found that UGI in Montreal could reduce air temperature by 4°C at tree level (i.e., 20 m above the ground), and by 2°C at greater heights (i.e., up to 60 m above the ground). Different water body types have various UBS cooling effects: for example, a 22-m-wide river was found to cool waterfront streets by 1.5–2.0°C [22], while other kinds of waterfront land use may be differently affected. Moreover, UBS-driven temperature changes can extend from a waterfront across impervious ground surfaces to 400 m, across lawn and bare land 362.5 m and 262.5 m, respectively, and through forest and farmland to 462.5 m [10]. Waterfront open space has also been found to boost the airflow and cooling effects of UBS [23]. For example, lakes are highly beneficial for urban wind farms [15]. Conversely, due to the heat storage capacity and thermal inertia of water, it warms more slowly than its surroundings during the day. Similarly, its speed of cooling is also slower at night, so that rivers and lakes cause the nocturnal temperature to rise in urban areas [24]. However, the effects of UBS on the urban thermal environment are still poorly understood [13].

Both UGI and UBS can effectively reduce air pollution. With respect to the UGI, it has been shown that some air pollutants (e.g., SO₂, O₃, and NO_x) are absorbed physically through the stomata of green plants or the leaf cuticles of plants and trees [25], or biochemically degraded by various metabolic processes in tree leaves [26]. Nowak et al. found that green plants removed 238.4 tons/year of air pollutants in Tabriz, Iran [27]. In the context of UBS, air pollution is known to be negatively correlated with relative humidity, but positively correlated with temperature [28]. Thus, evaporation from water bodies can also effectively reduce nearby air pollution, thereby accelerating the sedimentation of particulate matter and restraining the secondary transformation of precursors to particulate matter [29]. Additionally, the cooling effect of water leads to a temperature difference between lakes and surrounding land, which generates an offshore lake breeze [30].

The efficiency of urban land use is closely tied to local patterns of economic development, thus expanding the area of green and blue spaces to mitigate the UHI is highly infeasible in urban areas. The most practical strategy is instead to maximize the cooling effects of the existing blue and green spaces [31][32][33], however, only a few studies have focused on this approach. In recent years, the importance of synergistic cooling effects (SCEs) for green-blue space planning has been identified. To reap the full benefits of UCIs in highly urbanized areas, a balance must be found between the requirements of green and blue infrastructural elements [14][34]. To this end, several optimized methods have been proposed for designing green-blue spaces to maximize UCIs in large-scale urban areas, including integrating the eco-systems of green lands and water bodies, limiting riparian development, creating artificial water bodies within parks, studding older districts with green land, setting green bands along roads in the prevailing wind direction, and adding “wedges” of green land on the edge of cities [10][31].

However, despite extensive discussions on the capacity of urban blue and green spaces to mitigate UHI, four essential long-term aspects have not been well addressed, as follows. (1) Although previous studies have focused on the UCI effect and the factors affecting standalone

green [11][12][18][33][35] and blue spaces [19][23][31][36], there have been very few observational studies of the integrated synergistic dynamics of co-existing green and blue spaces [37]. (2) Researchers have mainly focused on large-scale rivers and lakes and have proposed frameworks for urban green-blue space planning based on these results, in line with theories of landscape ecology and urban planning [1][31][37], but have neglected quantitative examination of how dynamic SCEs of micro-scale green-blue spaces can mitigate the UHI in regional thermal environments. (3) The scope of the UCI effect has been investigated [10], but the spatiotemporal variations of heat due to different types of waterfront land-use have not. (4) Few studies have explored the relationship between the tree species present in waterfront green infrastructure and the UCI effect, despite the fact that the UCI effect is known to be species-specific [33][38].

Against this background, this study is focused on quantifying the SCEs of urban green and blue spaces on the local thermal environment in a hot-humid climate by on-site measurements and computational fluid dynamics (CFD) simulations. Specifically, this study comprises: (1) investigation of the spatiotemporal variations between common land-use types (i.e., impervious surfaces, forest, and lawn) with and without water based on integrated synergistic dynamics observations; (2) quantification of the SCEs of urban blue and green spaces and measurement of the spatiotemporal mitigation of summer surface UHIs due to different land-use combinations; (3) utilization of a validated ENVI-met model to qualify the effect of different tree species in a waterfront forest on the SCE of green-blue space.

These key tasks were addressed by co-modeling the thermal benefits of green-blue space design with the effects of all other ecosystem services. The outcomes of this study will serve as a realistic reference for theory as well as practice in urban and regional planning regarding urban water bodies and landscape design. Additionally, they will contribute to further reducing air pollution, mitigating the UHI effect, and improving thermal comfort for urban residents.

2 Study area

This study was conducted in Palm Springs International Garden (29.72°N, 106.63°E), No. 88, Jinkai Avenue, Yubei District, central Chongqing, China, as shown in Figure 1. The garden covers an area of approximately 1,200 acres, including approximately 160 acres of blue space. Although most of the site consists of open space with a relatively large water area, the terrain is undulating and the site is predominantly downwind of a high barrier formed by a mountain and several buildings, which may have a significant effect on the surrounding wind environment. Chongqing has a hot-humid climate with wet but very hot summers, and mild and wet winters, such that the relative humidity is greater than 70% in all months: the mean annual relative humidity is 78.9% and the maximum relative humidity is 85.9%, in December [39]. The annual mean temperature is 18.6°C and the maximum outdoor air temperature is up to 28.5°C higher in summer than in winter, ranging from approximately 7.5°C in December to 35.8°C in June. Solar radiation is much greater in summer, ranging from 121.2 W/m² in January to 558.8 W/m² in September [40][41].

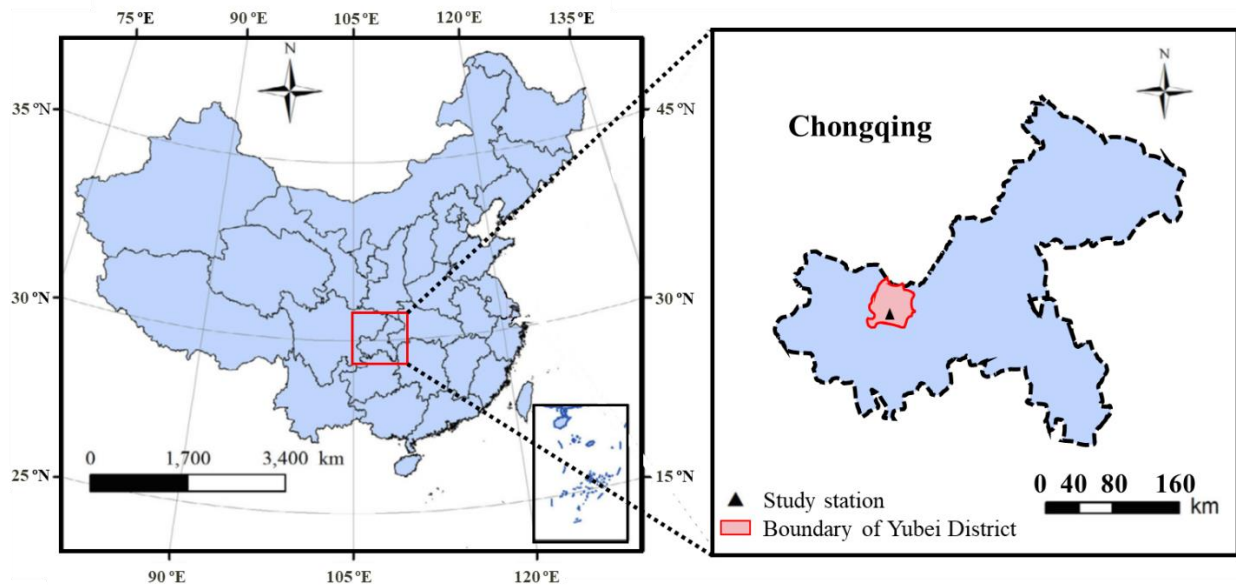


Figure 1. Location of study area and meteorological station.

3 Methodology

3.1 Methodological framework

The methodological framework of this study is shown in Figure 2. The study area contained 18 observation sites, comprising 15 sites with water and three without water (Figure 3). We conducted a field survey to characterize the built environment of the study area (i.e., the landscape cover and land use, i.e., green and blue infrastructure, impervious pavement, buildings, and constructions) and then built and parameterized the models using ENVI-met V4.4. On-site measurements of the park and area C (Figure 3) were used to calculate the spatiotemporal characteristics of the SCE. Furthermore, the observed air temperature (T_a) and relative humidity (RH) were compared with the results predicted by ENVI-met to validate the simulation performance. Additionally, the leaf area index (LAI) parameters of four locally common tree species were added to the database of ENVI-met, and simulations including each of these four species were conducted to predict how the LAI of vegetation affected the waterfront thermal environment. The simulated results were compared with those from the control group, which comprised a simulation of the basic case devoid of the landscape parameters of waterfront areas. Finally, conclusions were drawn and practical guidelines for landscape designers and policymakers were prepared.

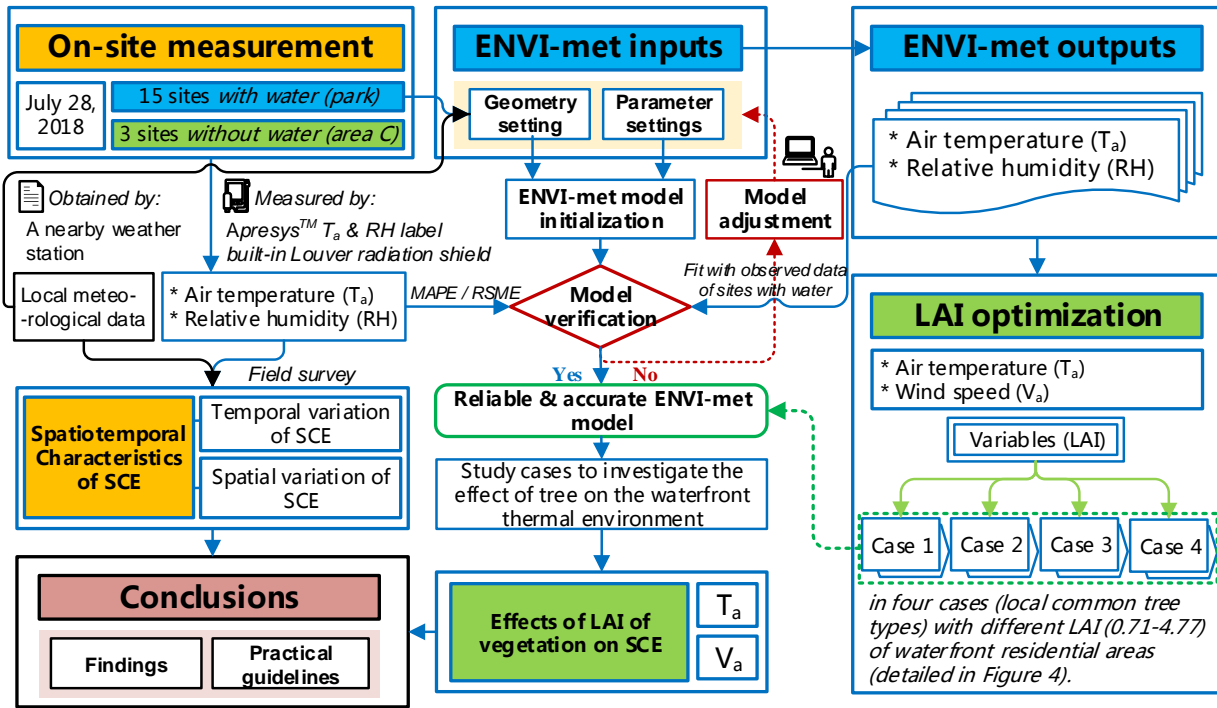


Figure 2. Flow chart of the overall study.

3.2 On-site measurement

To investigate the SCEs of urban blue and green spaces on the UHI, microclimate, and outdoor thermal comfort in a representative urban environment in summer, field observations were simultaneously carried out in a low-density residential neighborhood and an urban park. The observations were made during clear and windless days from July 1 to September 1, 2018. According to previous studies, the mitigating effects of water evaporation on the T_a and RH generally extend to a distance of 20.0 m from a blue-space border [42]. Sites 1–5 (in “Park” area), 6–10 (in area A), and 11–15 (in “Park” area) were located on a waterfront pavement of impervious material, or in a forest, or on a lawn, all of which contained additional water features, while sites 16, 17, and 18 (in area C) were on a pavement, or in a forest, or on a lawn, all without additional water features (Figure 3). The testing sites were arranged according to the JGJ/T 347-2014 Standards for Testing Methods of Building Thermal Environment and relevant provisions of the Code for Surface Meteorological Observations.



Figure 3. The location and general view of the study area (A represents the waterfront low-rise residential building area, B represents the waterfront villa area, and C represents the high-rise building area).

The on-site measurements were simultaneously performed at the pedestrian level (i.e., 1.5 m above the ground) using micrometeorological stations equipped with Louver radiation shields, where these stations contained a built-in thermistor temperature sensor connected to a data logger with an accuracy of 0.1°C along the measurement route. The T_a of each site was automatically recorded at 5-min recording intervals. Sites 1–15 were located on the waterfront pavement, or in a forest, or on a lakefront lawn at distances of 0.5 m, 3.0 m, 7.0 m, 12.0 m, and 20.0 m from the lake. Figure 4 shows the layout of the three sets of measurement points in the eco-park, and Table 1 illustrates the landscape parameters for each individual measurement site within the study area. Each set of measurement points was arranged radially, according to the direction tangential to the contour of the water body, although the actual arrangement of the measuring equipment was partly dictated by the greatly undulating ground. Wind speed and

direction were obtained from the micrometeorological stations nearest the measurement sites. In most cases, the wind did not change significantly during any given measurement session.

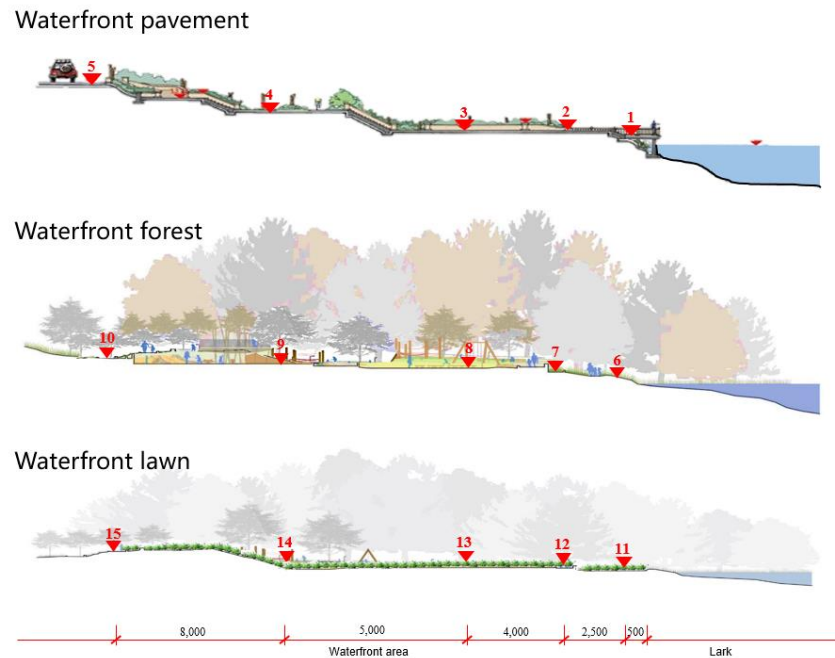


Figure 4. Profile of SCE measuring points and the general study area.

Table 1. Landscape parameters for each individual measurement site of study area

Site	Area	Distance from water (m), or location type	Landscape cover	With or without water
1	Park	0.5	Mainly concrete pavement, a few trees	With water
2		3.0		
3		7.0		
4		12.0		
5		20.0		
6		0.5	Residential street with greenery, urban park with lush forest	
7		3.0		
8		7.0		
9		12.0		
10		20.0		
11	0.5	A few trees and pavements, mainly grass cover		
12	3.0			
13	7.0			
14	12.0			
15	20.0			
16	Area C	Concrete pavement	Concrete pavement	Without water
17		Tree	Tree	
18		Lawn	Lawn	

Due to the large daily fluctuations of T_a , the data at 09:00, 14:00, 19:00, and 23:00 were selected to represent morning, afternoon, evening, and night time, respectively. In this study area containing a large lake, the different types of lakefront ground surface were widely distributed, and had markedly different cooling effects. Thus, to explore the effect of the waterfront environment on the UHI of the existing residential area in Chongqing, we compared the values of mean cool island intensity (MCII) to illustrate the cooling effect caused by different waterfront surfaces, as expressed in Equation (1) [7]:

$$MCII = T_0 - T_{Mi} \quad (1)$$

where T_0 represents the T_a derived from the nearby weather station located in an open space and T_{Mi} represents the average T_a of five waterfront sites at each time.

In addition, the correlation between the distance to the park and T_a was examined to clarify the total SCEs of the waterfront pavement, forest, and lawn on the surrounding area. Finally, the individual SCE was estimated by subtracting the cooling effect of water and land-types from the total SCEs. Here, the cooling effect of water was calculated as the difference between pavement sites with and without water, and the cooling effect of standalone land-type was calculated as the difference between pavement sites with and without water.

3.3 ENVI-met simulation

To investigate the local influence of different waterfront tree species on the waterfront thermal environment, the ENVI-met model v4.4.1 was used to simulate the microclimate of the Chongqing residential area containing the observation sites, based on synergistic dynamics. Figure 5 illustrates the simulation domain for field measurement and numerical modeling. ENVI-met uses statistically significant differences to estimate and compare the functions of underlying urban surfaces, buildings, and other infrastructure by combining the fundamental laws of fluid dynamics and thermodynamics into a holistic three-dimensional numerical model for urban microclimate simulation. The model can be updated dynamically according to thermal conditions,

and the driving forces of wind and solar radiation [43][44][45]. Additionally, the new ENVI-met model contains specialized 3D vegetation geometries and a “forestpass” function, allowing description of detailed forms, distributions, energy and mass balance of vegetation, and the turbulence properties of leaves. ENVI-met has been widely applied in evaluating the effects of urban green and blue spaces on the microclimate and thermal comfort in cities, and its performance has been validated in many places. Importantly, adjustments for the local vegetation geometries and underlying surface materials have been shown to further improve the model’s effectiveness [46][47][48].

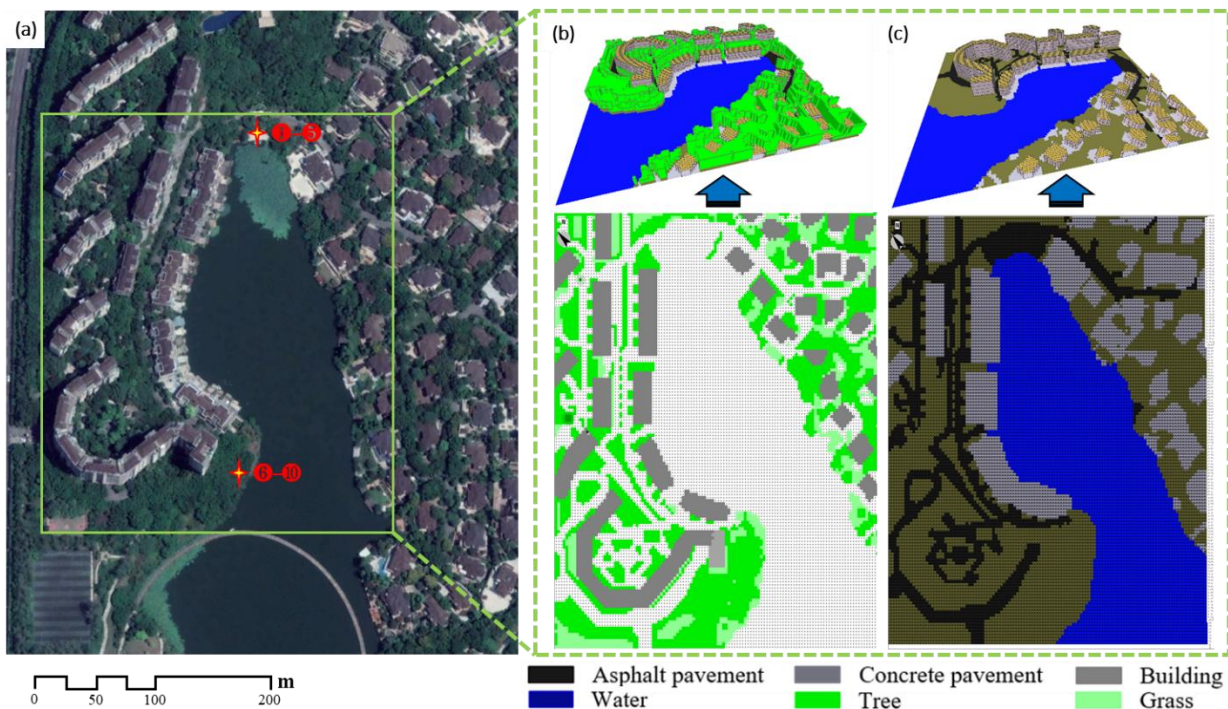


Figure 5. Geometric map and ENVI-met models of the study area and field measurement sites, where these are: (a) the chosen sites; (b) the land-use map of the study area in ENVI-met, and (c) a model without vegetation and other landscape parameters (control group).

3.3.1 Model setup and initialization

The model domain had an area of 198,400 m² (620 m × 320 m) and was modeled up to a vertical height of 90 m. The domain was characterized by densely placed low-rise residential buildings (on the west side of the lake), sparsely placed villas (on the east side of the lake), three impervious main roads, several side pavements, several types of vegetation, and a lake between two groups of buildings (Figure 5). The study area within this domain was divided into 120 × 140 square grids with 2.5 m resolution on the horizontal surface and 30 vertical telescoping grids with an initial resolution of 1.5 m and an extension factor of 20%. To minimize boundary effects, five nested grids were added to move the horizontal boundary away from the study area to ensure stability of the simulation. In addition, the model area was rotated 315° north, away from the grid, so that most façades were aligned parallel to the model structure.

Three-dimensional geometric information, dimensions of green and blue spaces and buildings, and a soil database were derived from Google EarthTM satellite images (captured on August 24, 2018), and on-site measurements. The building properties in the model were set up according to *JGJ26-2010 Design Standard for Energy Efficiency of Residential Buildings in Severe Cold and Cold Zones* (Table 2). The properties of urban natural elements and artificial surfaces are also shown in Table 3 [48][49]. Note that the original vegetation geometries built into ENVI-met relate to commonly found plants in high latitude countries such as Germany, with large leaves and high leaf area density (LAD). Zheng [50] summarized the commonly found plants in hot and humid areas of China (comprising six deciduous broad-leaved forests and nine evergreen broad-leaved forests in Chongqing) and found that the forests in these areas featured plants small in size and low in LAI (<5.0). In this study, therefore, seven typical plant species representative of each broad type of vegetation were chosen. Table 4 presents the properties of the dominant plant species in the simulation area. Aside from the height, crown diameter, albedo, and transmittance of a plant species, the LAD is a key parameter to describe the leaf distribution in the vertical direction. To estimate the morphological characteristics and energy balance of these

typical plants, the ENVI-met model was used to divide the plants into 10 layers and analyze the LAD in each layer by the following equation (Equation (2)):

$$LAI = \int_0^h L(z) dz = \int_0^h L_m \left(\frac{h - z_m}{h - z} \right)^n \exp \left[n \left(1 - \frac{h - z_m}{h - z} \right) \right] dz, n = \begin{cases} 6, 0 \leq z \leq z_m \\ 0.5, z_m \leq z \leq h \end{cases} \quad (2)$$

where L_m represents the maximal LAD and Z_m represents the height of the maximal LAD, m.

Table 2. Attributes of building roofs and walls

	Thickness (m)	Albedo (%)	Emissivity (%)	Heat capacity (J/kg·K)	Conductivity (W/m·K)	Density (kg/m ³)	Roughness (m)
Roof	0.30	0.5	0.9	1300	0.84	1900	0.02
Wall	0.30	0.3	0.9	1050	0.81	1800	0.02

Table 3. Attributes of ground profiles

Material	Thickness (m)	Heat capacity [L/(m ³ ·K)·10 ⁻⁶]	Heat conductivity (W/m·K)	Roughness (m)	Albedo (%)	Emissivity (%)
Soil		1.21	0.00	0.02	0.20	0.98
Water	3.00	0.00	0.00	0.01	0.00	0.96
Impervious	0.3	2.25	1.05	0.01	0.20	0.90

Table 4. The physical parameters of the plants within the study area

Type	Height (m)	Crown diameter (m)	LAI	Albedo (%)	Transmittance (%)
<i>Ficus microcarpa</i>	8.09	0.30	4.77	28.02%	9%
<i>Trachycarpus fortunei</i>	10.42	0.63	4.53	27.23%	11%
<i>Magnolia grandiflora</i>	6.75	0.14	2.83	27.61%	7%
<i>Bauhinia purpurea</i>	8.79	0.31	4.41	31.12%	8%
<i>Platanus orientalis</i>	11.34	0.57	0.71	29.32%	5%
<i>Ligustrum compactum</i>	5.51	0.20	2.19	30.01%	12%
<i>Cerasus yedoensis</i>	4.15	0.25	1.46	22.39%	13%

Moreover, to eliminate numerical instability, forced lateral boundary conditions were used to initialize the model. The meteorological data from on-site measurements and a nearby weather station were derived to initialize the simulation and to force hourly temperature and humidity profiles. Other relevant parameters were configured in accordance with the actual field status, as shown in Table 5. Initial wind direction and speed were set as 315° and 1.5 m/s, respectively. To overcome the influence of the initialization (6 h) and to reduce the computation time, the

simulations were started on a typical summer day, July 28, 2017, at 00:00 am for a continuous 24 h period.

Table 5. Initial parameters values for ENVI-met simulation.

Parameters	Definition	Value
Meteorological data	Wind speed, 10 m above ground (m/s)	1.5
	Wind direction (0°: N; 90°: E; 180°: S; 270°: W)	315°
	Roughness length (z_0) at reference point	0.01*
	Initial temperature of atmosphere (K)	Simple force
	Specific humidity at 2500 m (g/kg)	15.48*
	Relative humidity at 2 m (%)	94
	Initial soil temperature (K)	239
	Initial soil relative humidity (%)	60
Lateral boundary conditions (LBC)	LBC for temperature and humidity	Forced
	LBC for turbulence	Cyclic

Note: asterisked (*) parameters were sourced from the default values of ENVI-met v4.4.1.

3.3.2 Case studies

Five scenarios (Scenarios 1–5, comprising Cases 1–4 and the control group) were examined to investigate the effects of plants with different LAIs on waterfront microclimates and thermal comfort. The control group (i.e., the basic model, e.g., Figure 5 (c)) was configured without the vegetation inside the park region. Consequently, four simulation cases with vegetation were performed and the relevant microclimate data (T_a and wind speed) were obtained at 1.5 m from the ground. Figure 5 shows the spatial arrangement and LAI values of the five scenarios within the model domain. Four plant types (*Ficus microcarpa*, *Trachycarpus fortunei*, *Magnolia grandiflora*, and *Platanus orientalis*) were selected from Table 4. These four species of tree have relatively small differences in height, crown diameter, albedo, and transmittance, and thus the average values for each of these parameters (i.e., 9.15 m, 0.36 m, 28.04%, and 8.00%), were used for all four species. However, the four species differed significantly in LAI, and the T_a and RH differences between the tree types in both horizontal and vertical domains were estimated by Leonardo, the management function in ENVI-met for 3D microclimate simulation results. Accordingly, the net cooling effect and wind speed reduction in cases 1–4 were calculated as the

difference between the measured values for these two parameters in cases 1-4 and the simulated values for the control group.

4 Results and discussion

4.1 Model validation

Tsoka summarized 189 studies in which various climatic areas across the world were examined utilizing ENVI-met, and concluded that the model maintained high accuracy and reliability across diverse regions [51]. The ENVI-met simulations in this study area were conducted on the hottest day of the study period, i.e., July 28, 2018. To account for the complicated effects of underlying surface conditions, the T_a and RH from four representative sites 1.5 m above the ground – i.e., at site 1 (impervious pavement close to lake), site 5 (impervious pavement 20 m away from lake), site 6 (a plant close to lake), and site 10 (a plant 20 m away from lake) – were extracted for comparison with the measured data at these four sites.

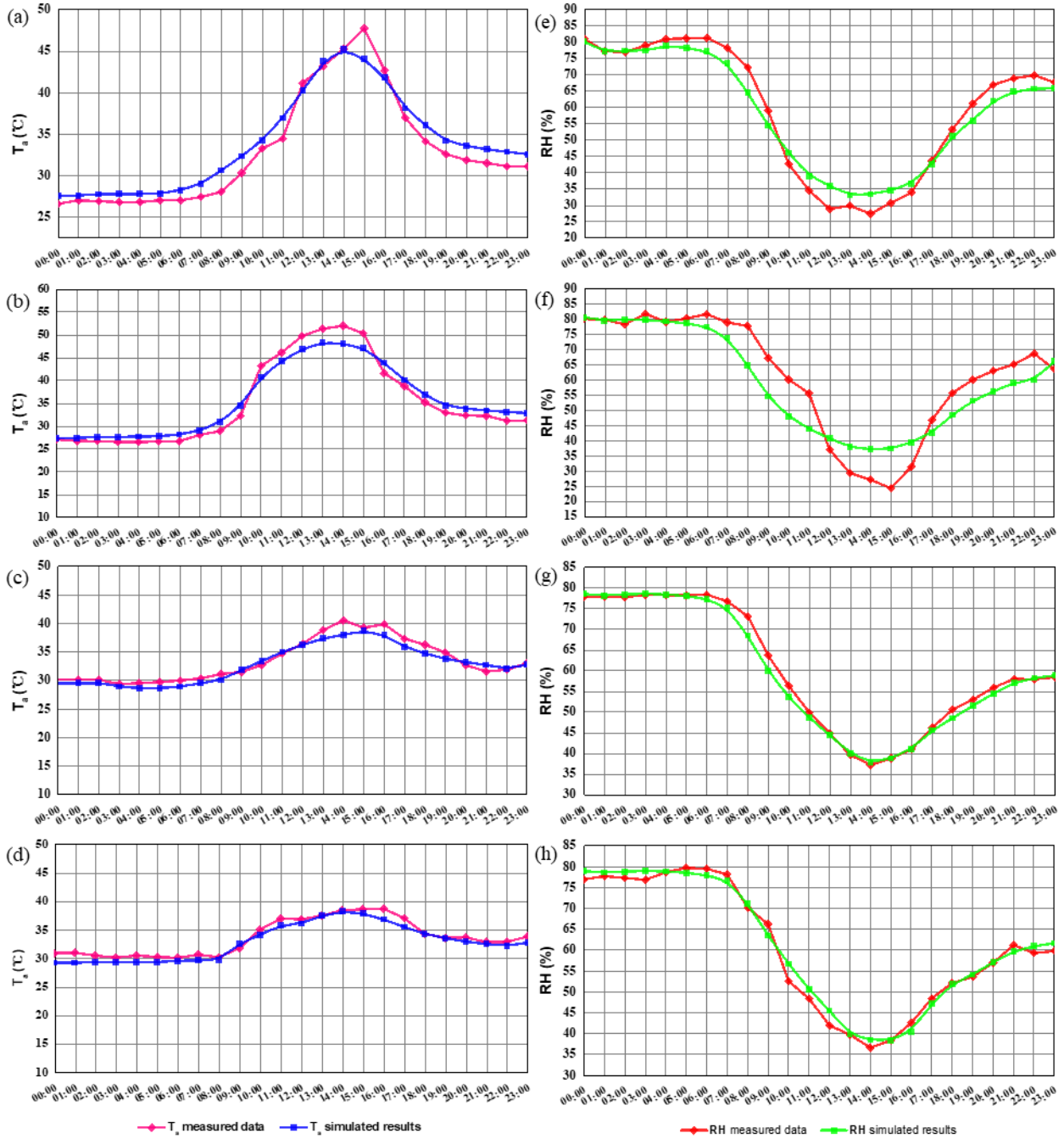


Figure 6. Comparison between measured and simulated values of (a)–(d) T_a , and (e)–(h) RH from 00:00 to 24:00 on July 28, where (a) and (e) are values for representative site 1, (b) and (f) are values for representative site 5, (c) and (g) are values for representative site 6, and (d) and (h) are values for representative site 10.

Figure 6 compares the measured T_a and RH at the four sites and the corresponding model results from 00:00 to 24:00 on July 28. The ENVI-met estimation outputs for the T_a are in good agreement with the observed value at each site, as shown in Figure 6 (a)–(d). T_a peaks in the afternoon: between 14:00 and 15:00, the observed T_a is between 47.7°C and 51.8°C, compared with ENVI-met-predicted values of 47.3°C and 47.8°C, at pavement sites 1 and 5, respectively. At sites 6 and 10, the measured T_a is between 29.3°C and 40.5°C and the ENVI-met values are 38.2°C and 38.7°C, respectively. Furthermore, as seen in Figure 6, good agreement also exists between the observed and the ENVI-met-generated RH results. RH reaches a maximum at approximately 06:00 for pavement sites 1 and 5, where the observed RH values range from 81.4–81.8% compared with ENVI-met estimations of 77.2–77.6%, while for sites 6 and 10 the observed RH values are 70.1–78.8% versus 70.1–79.0% as ENVI-met values.

To further evaluate the accuracy of the simulation, the root-mean-square error (RMSE) and mean absolute percentage error (MAPE) were selected to evaluate the validity of the simulating models. RMSE and MAPE are calculated by following equations:

$$RMSE = \sqrt{\frac{1}{N} \sum_{t=1}^N (T_{a,observed} - T_{a,predicted})^2} \quad (3)$$

$$MAPE = \sum_{t=1}^N \left| \frac{RH_{observed} - RH_{predicted}}{RH_{observed}} \right| \times \frac{100}{N} \quad (4)$$

These two indexes are used to measure the deviation between the observed value and predicted value, which can better reflect the actual situation of the error of predicted value. Lower values of RMSE and MAPE are indicative of better model performance. According to previous research on the accuracy of the ENVI-met model, an acceptable performance requires a T_a RMSE < 1.31–1.63°C, and an RH MAPE < 5.00% [51][52]. Table 6 presents the RMSE and MAPE for ENVI-met in the studied area. Overall, a strong agreement was found between the simulated results and the observed data, with RMSE and MAPE ranges of 1.02–1.95°C and 1.86%–4.94%, respectively.

Table 6. RMSE and MAPE of the ENVI-met model in the study area.

Error indices	Site	T _a (°C)	RH (%)
RMSE	1	1.58	
	5	1.95	
	6	1.12	
	10	1.02	
MAPE	1		4.94
	5		6.45
	6		1.86
	10		2.57

The ENVI-met microclimate model has been validated in a wide range of regions and cities [53][54][55]. In this study, ENVI-met was validated in Chongqing by comparing the measured data with the simulated results, and the accuracy and reliability were again estimated by RSME and MAPE. Although the error indices indicated an overall qualitative agreement with the measurements, the predicted T_a of all four sites were lower than the observed data in the daytime. Nonetheless, these values fell within the error band of the measured data (Figure 6). A similar trend was reported by Toudert [43]. Furthermore, the simulated results predicted the maximum T_a would occur approximately 1 h earlier than was actually observed (Figure 6). Notably, the prediction of RH has been identified as a common weakness of ENVI-met in many studies [52]. This implies the existence of flaws in the radiation model of ENVI-met, making it likely that the long-wave radiation from ground objects and the thermal stability of each underlying surface type in the study area would not be accurately simulated. This proved to be the case, with particularly large errors evident in data from site 5. We propose that the observed data were influenced by anthropogenic heat discharge, including human body-heat emission and heat from transportation modes, causing higher T_a and lower RH than predicted by ENVI-met. The simplified assumptions of the model may also have contributed to these errors.

4.2 Local thermal environment over green and blue spaces

4.2.1 Comparison of T_a profiles with and without blue spaces

Figure 7 compares the T_a trends between all sites with and without water on the hottest day, i.e., July 28, 2018. As expected, impervious pavement, which is one of the most common

underlying surfaces in urban areas, possessed the highest daytime mean T_a of 35.7–37.0°C, while the dense forest yielded the strongest cooling effect with a mean T_a of 30.6–34.1°C. The T_a range of the lawn sites was 35.7–37.8°C, these T_a are hotter than those for impervious pavement.

As is shown in Figure 6 (a), the warming effect of the unshaded pavement (site 16) is obvious: the daytime mean and maximum T_a are respectively 1.6–2.1°C and 1.7–5.3°C hotter than the observed data of the waterfront pavement sites 1-5. Additionally, the T_a at site 16 increases markedly from 8:00 to 12:00 and reaches a maximum at 14:00, while the T_a of waterfront sites reaches a maximum half an hour later. In contrast, the cooling effect of water evaporation significantly lowers the T_a of the waterfront pavement, an effect that gradually weakens with increasing radial distance. The maximum and mean T_a of waterfront pavement sites shows an upward trend, with a sharp increase from 50°C and 33.6°C at site 1 to 54.8°C and 35.7°C at site 5, respectively. At night these differences in T_a increase to 0.9–2.0°C and peak at 2.0–4.5°C.

At the waterfront urban forest sites 6–10 and the forest-only site 17, Figure 7 (b) shows that the T_a remains stable between 27.6 and 31.1°C at night, and then reaches a maximum at 14:30–15:00. Site 6 possesses the highest mean and maximum T_a of any waterfront forest site. It must be noted that site 6 was very close to the lake (i.e., 0.5 m away), where few trees were available for shading due to tree-felling activity. Accordingly, the mean and maximum T_a of site 6 are 36.6°C and 52.9°C, respectively, approaching those of the overall hottest site, site 16 (56.3°C and 37.0°C, respectively) and the second-hottest site, site 1 (51.0°C and 33.6°C).

The differences in T_a between forest areas with and without water remained large throughout the day, with a daytime mean T_a difference of -1.5–3.9°C, and a daytime maximum T_a of -13.6–5.6°C. Compared with forest-only sites, waterfront forest sites, excluding site 6, exhibited stronger cooling effects; the greatest cooling effect of 27.2–32.9°C was observed at site 8 (7 m from the lake), followed by site 7 (30.2–39.2°C), site 9 (30.8–38.5°C), and finally site 10 (31.1–37.8°C). A similar T_a variation between sites 10 and 17 demonstrated the importance of the evaporative cooling effect, which extended 20 m from the waterfront.

In contrast, the mean daytime T_a of the waterfront lawn, containing sites 11–15, was 0.8–2.1°C higher than that of the non-waterfront lawn site 18, and this difference increased to 2.6°C when compared with the daytime maximum T_a . The increase in T_a of waterfront lawn sites can be attributed to the presence of sunburnt grass and the sensible heat exchange effect of water, as the lake accumulates considerable heat in the daytime and then releases it after 15:00. Therefore, the waterfront lawn was 2.3–3.8°C hotter than the non-waterfront lawn between 15:00 and 20:00.

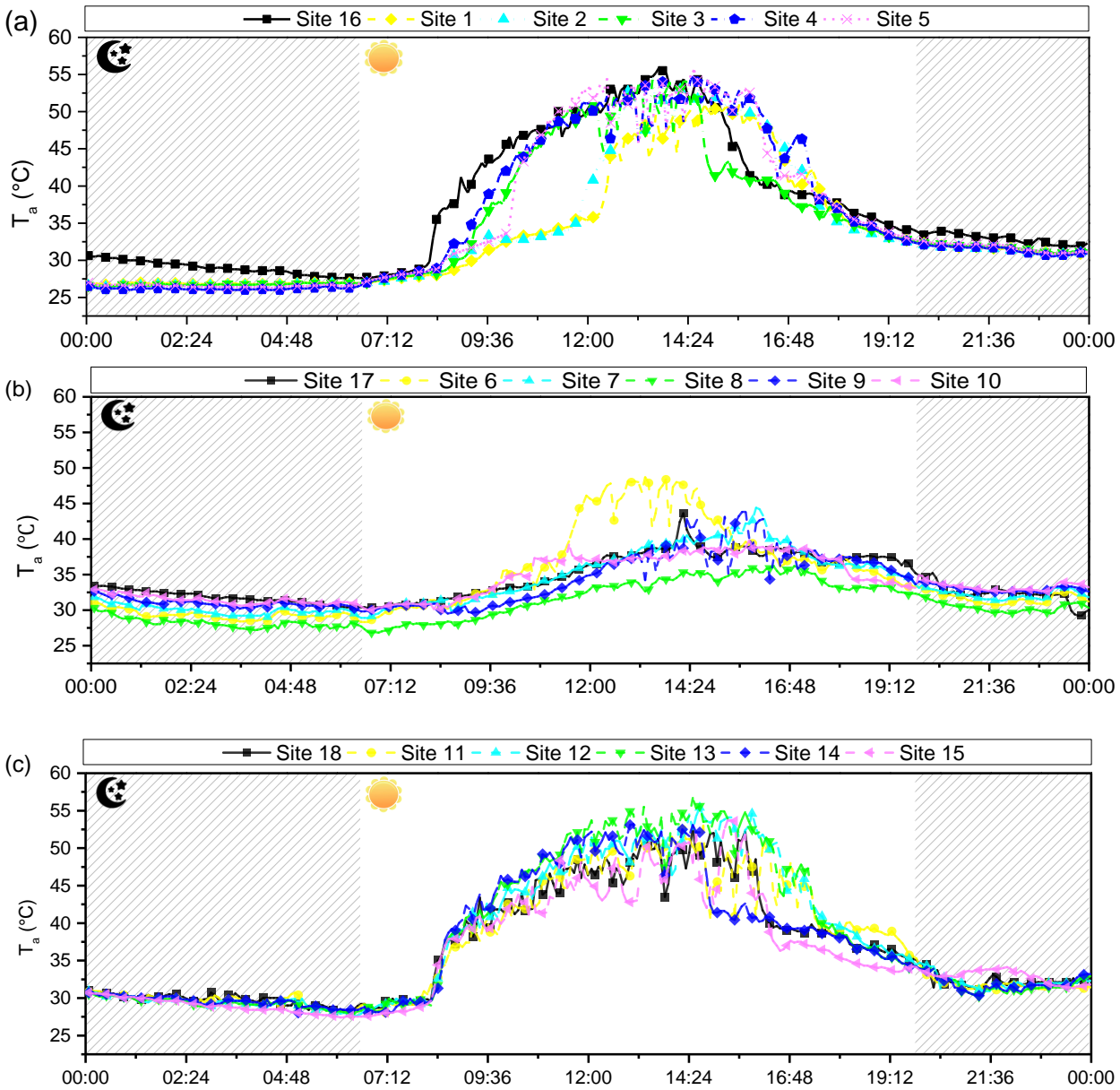


Figure 7. Comparison of T_a temporal changes between the observation sites with and without water on July 28, 2018: (a) pavement sites; (b) forest sites; and (c) lawn sites.

As is shown in Figure 7, the T_a of each observed site changes significantly throughout the day, and the study sites are not uniform in temperature. Hence, it was considered that the average temperature provided the clearest picture of the differences in measured T_a between specific underlying urban surfaces and the micrometeorological parameters from a nearby weather station. Figure 8 compares the average T_a for three typical underlying urban surfaces with the T_a from a nearby weather station at 09:00, 14:00, 19:00, and 23:00. As can be seen, the T_a of waterfront forests is significantly lower than that of surrounding urban areas throughout the day, corresponding to MCII values of 9.62°C, 7.54°C, 1.30°C, and 0.30°C at 09:00, 14:00, 19:00, and 23:00, respectively. These results indicate that waterfront forests can mitigate the UHI effect throughout the day. Meanwhile, it can be seen that the waterfront lawn reduces the UHI effect by 1.92–7.23°C at most times, but aggravates it at 14:00 (MCII = -3.76°C). Finally, waterfront pavement exacerbates the UHI effect during the daytime, but has a small cooling effect (MCII = 0.52°C) in the evening.

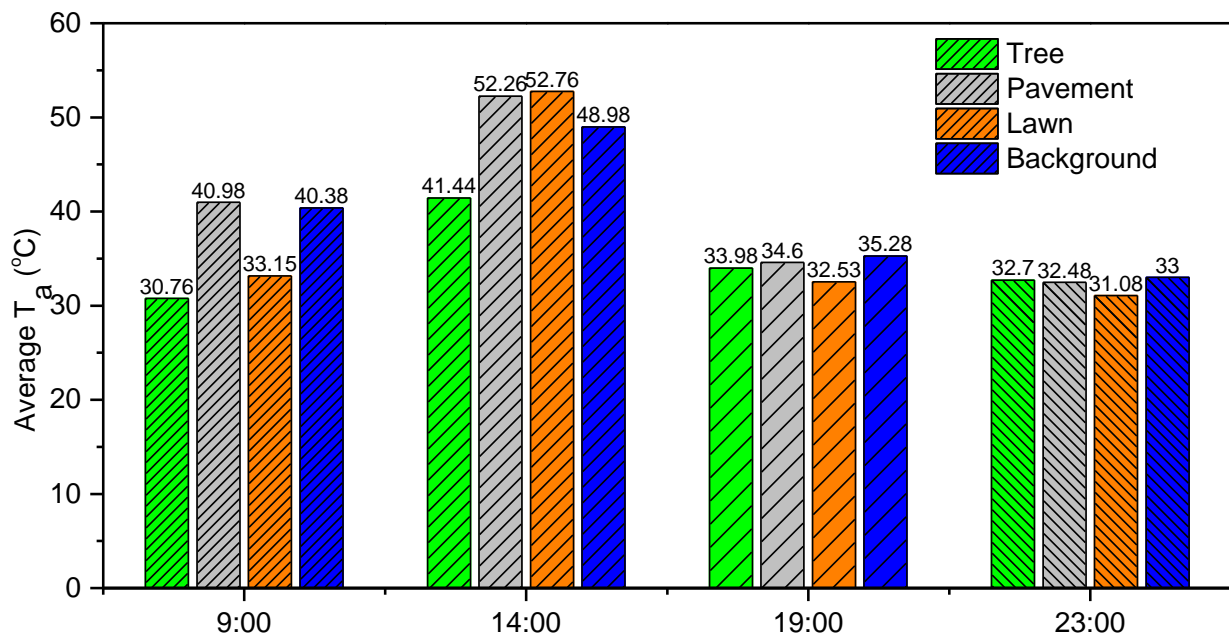


Figure 8. Comparison of average T_a of waterfront forests, pavement, and lawn with those of a nearby weather station at 09:00, 14:00, 19:00, and 23:00.

4.2.2 Spatial variation of air temperature over waterfront sites

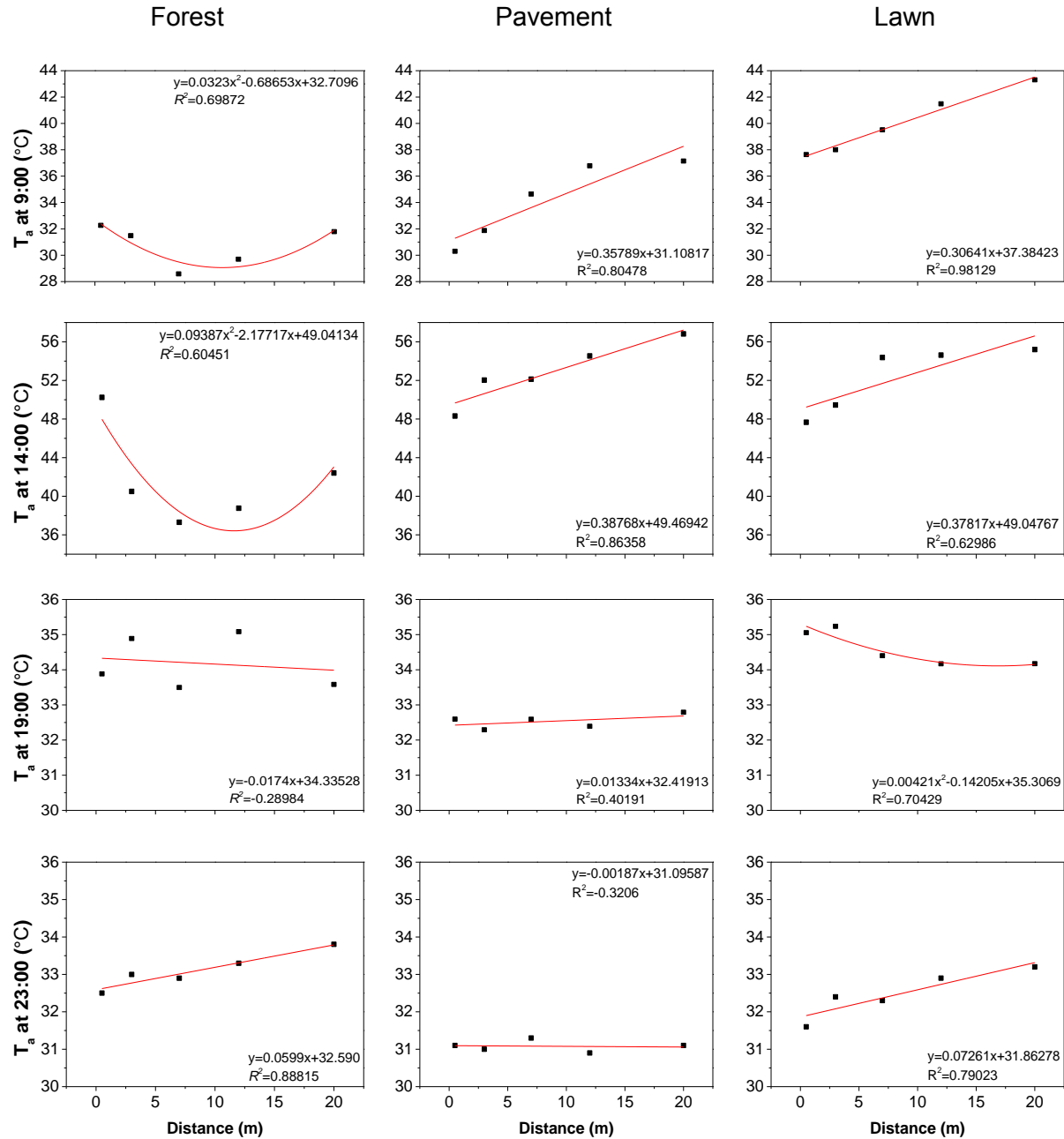


Figure 9. Relationship between the distance from the lake and T_a for every measurement site (i.e., impervious surfaces, forest, and lawn).

Figure 9 shows the spatial distribution of T_a at waterfront forest, pavement, and lawn sites at 09:00, 14:00, 19:00, and 23:00, and the relationship between distance from the lake and T_a for each observed site. Both heat inertia and the distance to water cause the differences in the T_a distribution at the waterfront sites that have various underlying urban surfaces. Figure 9 indicates that at 09:00, 14:00, and 23:00, the cooling effect weakens as the distance from the lake border increases, and that from morning to night, the T_a of the waterfront pavement and lawn increases while that of the forest first falls and then rises. Furthermore, the strongest cooling effect is that of the waterfront forest in the daytime, while the waterfront forest and lawn have a higher T_a than the waterfront pavement from evening until night.

In the daytime, for the waterfront forest, as the distance from the lake increased the T_a decreased to a daytime minimum, before rising until the end of the day. These SCEs of the forest and lake was particularly evident at approximately 10 m from the water at solar noon (14:00), when the coefficient of determination R^2 was 0.605. For waterfront pavement and lawn surfaces, a similar T_a variation was observed: as the distance from the lake increased, the T_a continuously increased; the cooling effect of water evaporation was most significant at 14:00, when R^2 was 0.864 and 0.630 for pavement and lawn, respectively. For each 1 m increase in the distance from the lake, the T_a increased by approximately 0.39°C and 0.38°C for pavement and lawn, respectively. In addition, buildings shaded the waterfront pavement in the morning, resulting in T_a at this location being 4.5–5.5°C lower than that of the waterfront lawn. The differences in the spatial distribution of T_a indicate that the urban surface characteristics surrounding blue space significantly influence the cooling range and intensity. For the waterfront forest, the shading effect and heat inertia of trees generated for evaporative cooling, contributing to the significant cooling intensity of this landscape type. However, a high density of trees causes airflow shielding, especially if these are tall trees, which limits the extent of spatial penetration of the cooling effect of green-blue spaces into the urban environment. Therefore, enhanced cooling extends only a relatively short distance beyond the perimeter of the waterfront forest.

In contrast, the warming effect of heat release from water was obvious: at 19:00 the T_a decreased with increasing distance from the lake margin. The R^2 value for this effect was 0.290, 0.401, and 0.704 for forest, pavement, and lawn, respectively. For each 1 m increase in distance away from the lake, the T_a decreased by approximately 0.02–0.03°C. Due to their greater heat storage capacity, the T_a of forest and lawn were 1.3–1.8°C higher than that of the pavement, which remained at approximately 32.5°C. At 23:00, T_a began to increase as the distance from the lake margin increased, indicating that the release of heat stored in the daytime was almost complete. Specifically, with increasing distance from the lake, the T_a of the forest and lawn continuously increased by approximately 0.06°C and 0.07°C per unit distance, with R^2 values of 0.888 and 0.790, respectively. However, due to the greater heat inertia of vegetation compared with pavement, the T_a of forest and lawn were 1.5–2.7°C higher than that of hard road surfaces, and the temperature in the waterfront plaza remained approximately 31.0°C.

4.2.3 Temporal variation of synergistic cooling effects (SCEs)

By measuring the spatial distribution of T_a surrounding the lake, it was found that the green and blue spaces exhibited a significant SCE, owing mainly to the combined influences of water evaporation, shading, and improved heat inertia. The SCE was estimated by subtracting the individual cooling effects of water and forest from the total cooling, where the cooling effect of water was calculated as the temperature difference between pavements with and without water, and the cooling effect of forest was calculated as the temperature difference between forest with and without water. Figure 10 shows that after subtracting the cooling effect of water, the remaining T_a reduction of waterfront forest was still higher than that of forest without water, where the red grating area represents the SCE between 12:00 and 15:00.

These results implied that the SCE of the forest and lake occurred at some distance from the water; i.e., as can be seen in Fig. 10, as the distance from the lake border increases, the SCE increases for approximately 5.0 m, peaks at approximately 7.0 m, and finally decreases at 12.0–

18.0 m. The cooling effect of water evaporation is most significant at 14:00, being approximately 4.3°C. Notably, the T_a reduction of the non-waterfront trees falls to approximately 10°C at 14:00, possibly because a photosynthetic “noon break” occurs at this time [7]. After the peak, the SCE gradually weakens as the T_a decreased, and drops to 3.3–5.0°C at 15:00. Additionally, due to the lack of shading in site 6 (0.5 m away from water border), worse cooling effect was observed in site 6, T_a reduction of site 6 was approximately 10 °C lower than that of site 17. This lack of shading is unavoidable in Chongqing, as the serious soil erosion, shallow, thin soil is commonly mixed with large quantities of shale or mudstone debris in this city, fewer trees are planted close to the water border [56].

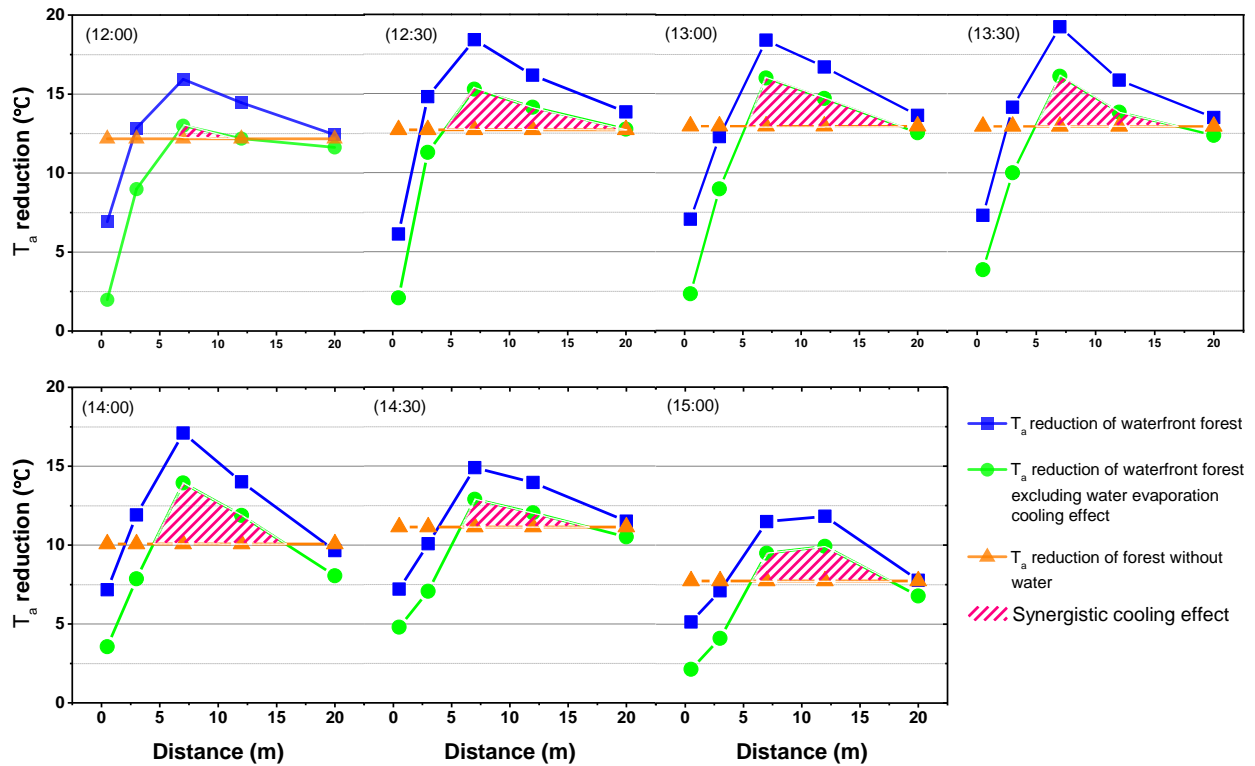


Figure 10. The SCEs of green and blue spaces between 12:00 and 15:00.

4.2.4 Effect of tree species with different LAI on the waterfront thermal environment as measured by T_a

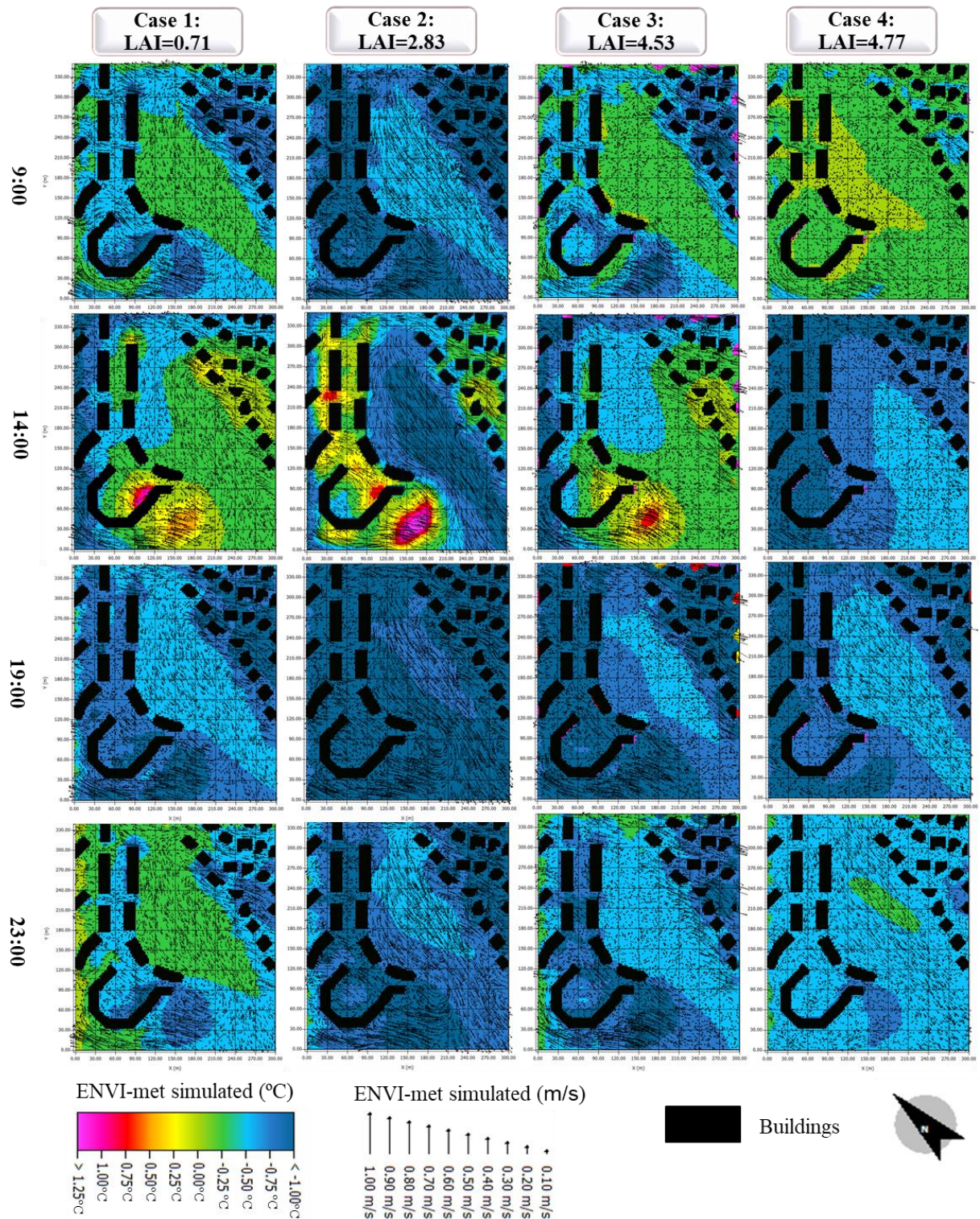


Figure 11. Simulated values of T_a and wind speed reduction in four cases at 09:00, 14:00, 19:00, and 23:00.

Figure 11 shows the regional cooling effect and wind speed reduction of the four cases. It is evident that T_a is effectively reduced by the waterfront forest, i.e., vegetation significantly improves the waterfront thermal environment, compared with the control group without UGI. It can be seen that the cooling effect of the waterfront forest is greatest in the evening and night, followed by the afternoon, and smallest in the morning. The T_a reduction by Case 1 (1.18–2.38°C) is significantly better than that of Case 2–4 (0.26–0.71°C) at 14:00, 19:00, and 23:00. Conversely, at 09:00, Case 1 (regional average reduction of 0.17°C) displays a weaker cooling effect than Case 2–4 (0.25–0.41°C), and Case 3 performs the most apparent cooling intensity.

In addition, the waterfront green infrastructure has different cooling effects on the three waterfront building groups with different layouts, with the effect being greatest for multistory residential buildings located west of the lake. The regional average T_a reduction range is 0.12–0.34°C at 09:00, and reaches 0.74–2.15°C at 19:00. For the waterfront villa area located east of the lake, at 09:00, the cooling intensity of waterfront green spaces is the smallest of all, ranging from 0.06 to 0.28°C. At 19:00, the cooling effect in this area is at a maximum; the greatest cooling intensity is 1.56°C, with an average of 0.33°C.

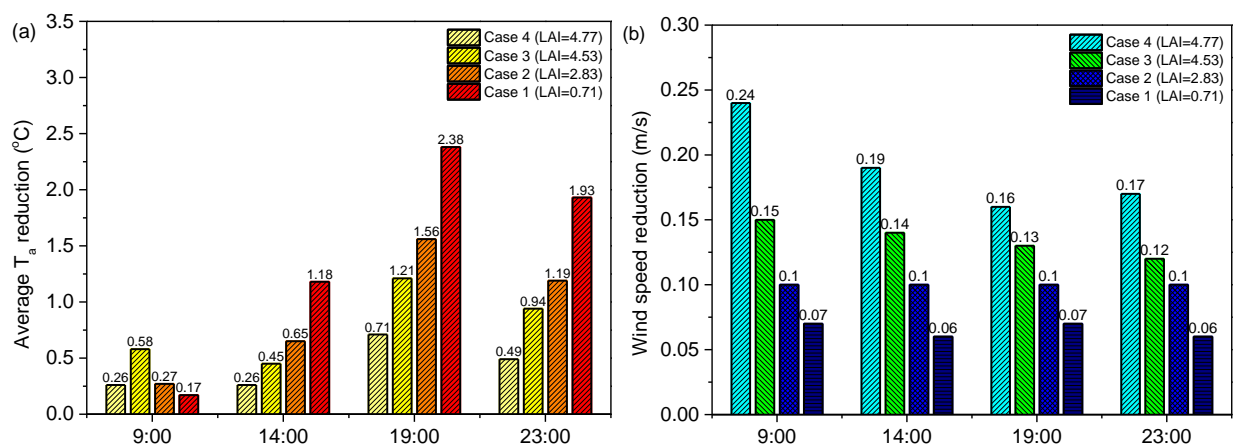


Figure 12. The average regional (a) T_a and (b) wind speed reductions of four cases at 09:00, 14:00, 19:00, and 23:00.

Figure 12 depicts the statistical analyses of the average regional T_a and wind speed

reductions in the four cases at the four representative times. The higher the regional T_a reduction, the weaker the wind flow, the smaller the LAI, and the more obvious the SCE. Furthermore, the larger the LAI, the greater the canopy resistance and the more obvious the wind velocity attenuation, as seen in Figure 12 (b). It can be seen that the average regional T_a reductions by the four species are lowest at 09:00, while the regional cooling effects generally decrease with increasing LAI. However, the attenuation of wind flow peaks at 09:00 (0.07–0.24 m/s). Case 2 shows the greatest T_a reduction at this time, 0.58°C, and again at 14:00 and 23:00 when the cooling intensities are 0.26–1.18°C and 0.49–1.93°C, respectively. Meanwhile, the wind speeds decrease by 0.06–0.19 m/s at these times.

The cooling effect is most pronounced at 19:00, when the mean cooling intensity is 0.71–2.38°C. Meanwhile, the smallest attenuation of wind occurs at this time, being 0.06–0.16 m/s. Conversely, it can be seen that from afternoon to night the regional cooling intensity of the waterfront forest improves as the LAI decreased, and the gap in UCI ability between the four species widens. When the LAI decreases to 1.0, the average cooling effect increases by 0.19–0.31°C. At night (23:00), the lake dissipates heat to the surroundings due to its relatively high temperature, and the very low wind speed hinders the convection and heat dissipation of water. This leads to intensified heat conduction from the lake to the interior of the residential area, weakening the cooling effect of the area with high-LAI plant coverage.

4.3 Discussion

4.3.1 SCEs of urban green and blue spaces on the local thermal environment

Urban green and blue spaces are considered important UHI mitigation strategies [54][55][57], however, comparative assessment of their combined effect in different regions and cities is rare. Therefore, in this study, the spatial distribution of T_a throughout waterfront forest, lawn, and pavement environments in Chongqing was observed by on-site measurements. Then, the integrated dynamics of heat reduction between green and blue spaces were investigated and

analyzed. The results indicated that during the daytime, the T_a of forests was approximately 1.6°C and 2.9°C lower than those of lawn and impervious pavement, respectively. The dense vegetation of the forest and greater heat release from anthropogenic components in urbanized sites are potential reasons for the lower temperature found in the former [14][58][59]. Additionally, lower T_a was observed at the waterfront sites than at the sites without water. Meanwhile, the variation in the daytime mean T_a was relatively small at the waterfront sites. This indicates that water evaporation contributed to the stronger cooling effect in the waterfront thermal environment, which probably represent SCEs of the local water body (lake) and plants [60].

Furthermore, the lake improved the climate resilience of waterfront environments in the daytime, and not only strengthened the cooling effect by 1.2–3.4°C but also prolonged the cooling period by 0.8–21.0%. However, as the heat inertia and capacity of vegetation are much higher, the downtrend of T_a showed thermal hysteresis in the afternoon, concurrent with the heat release from the water body. The T_a of the waterfront forest and lawn were significantly higher than that of the non-waterfront forest and lawn between 17:00 and 20:00, while the greatest warming effect of at 2.3–3.8°C was observed in the waterfront lawn. This indicates that both cooling and heating effects were still significant even far downwind; similar results were reported by Akio in Nagoya [61], where a difference of 3.0°C was measured among downwind waterfront areas of different types.

However, the cooling intensity of the study area showed clear temporal variation. The study area's MCII was not significant at 14:00 (7.54°C for forest, -3.82°C for pavement, and -3.78°C for lawn), this is consistent with Yan's study in Beijing, which found that the cooling effect of an urban park in terms of UHI mitigation was lowest at 14:00 (0.6°C) [7]. At 23:00, the cooling effect was 0.91°C, while at 19:00, the cooling effect was higher at 1.58°C (1.30°C for forest, 0.68°C for pavement, and 2.75°C for lawn) owing to the heat release and residents' outdoor activities. Finally, the most pronounced cooling intensity was approximately 5.42°C at 09:00 (9.62°C for forest, -0.60°C for pavement, and 7.23°C for lawn), considering the intense anthropogenic heat

discharged by transportation at this “rush hour” time, the T_a value at 09:00 would have been much higher without the effect of the park.

In contrast, Jauregui studied the cooling effect of a large urban park (without water) in Mexico. It was found that the park had the largest cooling effect at night because its cooling rate was even greater after sunset, reaching 3–4°C [62]. Consequently, it was concluded that blue space can improve the heat inertia of surrounding green space, reduce the peak temperature, and significantly lower the heating rate in the morning. Notably, the combined cooling effect of blue and green spaces was recorded as 5.42°C, compared with 3.6°C for parks and 2.9°C for lakes alone, according to a comparative assessment of six parks and three lakes in Chongqing [8].

In previous research, synergistic cooling was principally recommended as an achievable future improvement based on established principles, or regarded as a hypothetical explanation for anomalously high cooling enhancements [38]. The shading effect of waterfront greening extends to the surface of the water, weakening the solar radiation that enters the water body. In this study, the SCE was preliminarily estimated by subtracting the isolated cooling effects of the vegetation and water body from the total cooling; the results showed that the cooling extended 7–12 m further than that of a separate (non-waterfront) green space, and was more than 3.3°C in the daytime. It is found that the SCEs are more than cooler T_a of green-blue spaces than standalone green/blue space. In the daytime, the SCEs of green-blue spaces yielded 3.3°C more cooling intensity than standalone forest. It is possible owing to good ventilation and effective evapotranspiration. Conversely, the heat release of water body at night may warm the surrounding air. SCE is embodied in the concept of ‘blockage effects’ of the warm land-water breeze by trees at night, the SCEs of waterfront forests were most pronounced at 19:00, with a T_a reduction of 0.71–2.38°C in the four cases compared to the baseline scenario.

As the distance from the lake border increased, the waterfront forest became denser with a less regular array of trees. Thus, with increasing distance, the shading effect of trees was

enhanced and their regulating effect on the temperature was greater. At observation site 15 (20 m from the water), the cooling effect was similar to site 17, which indicates that the cooling effect of water on waterfront trees extended less than 20 m. However, the T_a of site 5 on the waterfront pavement was still 1.3°C lower than that a site 16. This revealed that the cooling effect of water on the pavement extended more than 20 m.

4.3.2 Influence of tree species on the blue space at daytime and night

Previous studies have demonstrated that blue spaces improved the thermal comfort of urban environments, particularly in the daytime [22], and have confirmed that blue spaces had a cooling effect [63]. The T_a of the study area herein was further reduced via the SCEs of green and blue spaces, and different LAI-type trees showed significantly different effects (Figure 11). When high-LAI trees were present, the cooling effect of the water body failed to extend inside the residential areas, and the T_a differed markedly between the interior of the residential areas and the waterfront area. Trees with a higher LAI thus showed a lower cooling effect in the study area, although the variation in the T_a reduction as a function of tree type was smaller in the daytime. This latter effect was probably an example of SCE interactions between the local geography and plants, i.e. local geography acted as windshields in the park during the daytime, thus further reducing the cooling effect of both high-LAI and low-LAI waterfront trees [60]. In contrast, low-LAI trees displayed more pronounced SCEs with green and blue spaces and their cooling effects extended inside the residential areas in the afternoon. By improving the effect of water cooling, low-LAI trees showed stronger SCEs with blue spaces than did high-LAI trees. However, in the morning, the contribution of water evaporation to regional T_a reduction was smaller; hence, the shading function of dense trees resulted in their having a stronger cooling effect than low-LAI trees at this time of day [8].

It was previously found that at low altitudes, UBS had a significant UCI effect during the day, but could warm the surrounding air at night, possibly due to the temporal variation in the evaporative flux [15][38]. Considering the high heat storage and thermal inertia of water, green-

blue space can be regarded as a thermal buffer, which not only suppresses the peak value of air temperature, but also moderates its temporal variations. Blue spaces release heat at night to limit nocturnal cooling [24]. However, waterfront trees can isolate the heat released from hotter blue spaces at night and prevent residential areas from heating up. Compared to high-LAI trees, low LAI trees could promote the blue space to dissipate heat at night, as high LAI trees attenuated blue-space wind velocity less than did low-LAI trees.

Overall, although our results highlighted the waterfront forest as a way to provide SCEs – that is, further reduce the T_a of the waterfront thermal environment and urban microclimate – it is important that the forest should not be too dense, so that heat release from blue spaces at night is moderated and the T_a in residential areas does not rise to an intolerable level.

4.3.3 Air pollution control

The use of urban green-blue space can improve air quality by reducing ambient temperature, increasing humidity, and reducing wind speed to reduce the concentration of air pollutants [28]. Herein, at 9:00–17:00, the green-blue space has apparent SCE within 7–12 m from the lake border (Figure 9), where the mean T_a reduction is 3.3°C higher near a waterfront urban forest than the sum of the cooling effects of standalone water and forest. Forests can constrain the wind velocity to a certain range, not only scattering airborne particles widely on the leaves, but also preventing the diffusion of air pollutants [27]. Although the shielding effect of high-LAI trees reduced the effect of water cooling inside the residential area, the trees with larger LAI herein (0.47–0.71) achieved more obvious wind velocity attenuation (0.06–0.19 m/s). Moreover, the cooling effect of water leads to a temperature difference between lake and land, which will create an offshore lake breeze. Then the transports pollutants to the surface of the water body where they are captured by subsidence airflow, thereby promoting air purification [64]. Therefore, theoretically, a combination of green and blue spaces can further reduce the air pollutant.

4.3.4 Practical guidelines for urban design strategies

This study has revealed that green spaces connected with blue spaces intensify each other's UCI effects and improve the outdoor thermal environment [5][65]. Therefore, waterfront forests may have a significant effect on urban landscape planning and construction [36]. On a summer day, the waterfront forests displayed obvious SCEs within 7–12 m from the water's edge, where the T_a was lower than that of the non-waterfront forest by approximately 3.3 °C. Therefore, to decrease the UHI intensity and improve human thermal comfort, it is recommended that forest trails or sitting areas are introduced within waterfront forests, if possible, rather than on pavements or lawns far from water. On the summer day of this study, the trees with smaller LAIs produced a higher local T_a reduction. When the LAI decreased by 1.0, the average cooling effect increased by 0.19–0.31°C. Therefore, to improve UHI mitigation and urban landscape design, it is suggested to consider trees with lower LAIs when planting forests, so as to improve the regional cooling effect.

The cooling effect of water evaporation improved the thermal inertia of waterfronts, protecting against extreme weather situations [38], and not only enhanced the cooling effect, but also prolongs the duration of cooling by the waterfront. However, the warming period at the waterfront was also prolonged due to the heat release from water at night. Therefore, it is recommended that trees with smaller LAIs are planted around blue spaces. Trees can isolate the heat released from hotter blue spaces and prevent residential areas from heating up at night, and trees with lower LAI can achieve this more efficiently because they have less effect on the wind velocity.

5 Conclusions and future work

This study investigated the potential of SCEs from urban green and blue spaces to improve the local thermal environment of residential surroundings in a hot-humid city. From the observational results, it was found that waterfront environments were significantly cooler than the corresponding sites without water during the daytime, but slightly warmer at night owing to heat

release. Due to the thermal inertia of the water, the temperature of the waterfront forests, lawns, and plazas changed more gradually during the day; the peak value decreased and the time of peak temperature lagged behind the non-water case. A significant reduction in the mean and maximum T_a (1.85°C and 3.50°C, respectively) was observed in the waterfront forest, followed by waterfront impervious pavement (1.80°C and 2.1°C, respectively). However, the waterfront lawn was actually 0.8–2.1°C hotter than the non-waterfront lawn, which indicates that lawn is unsuitable for waterfront areas.

The cooling intensity was prominent not only within the border of the blue space but also extended to approximately 20 m away. The waterfront forest was identified as providing significantly greater cooling effects than other surrounding land-use types, including waterfront lawn and pavement. The MCII of the study area was largest in the morning, due mainly to the effect of the waterfront forests. This provided evidence that the SCEs of green and blue spaces can better stabilize the fluctuation of temperature than other urban infrastructures. The air temperature first fell and then increased with increasing distance from the lake. Hence, the SCE was most effective at 7–12 m, where the T_a reduction of waterfront forest was higher than the sum of the separate forest and water terms by approximately 3.3°C in the daytime.

Furthermore, this study revealed the SCEs of green and blue spaces on the thermal environment of waterfront areas, and also found that tree species with low LAI had a greater cooling effect on the surrounding waterfront thermal environment. Specifically, when the LAI decreased by 1.0, the average cooling effect increased by 0.19–0.31°C. At night, water bodies can warm the surrounding air as a result of heat release. Through the blockage of the warm land–water breeze by trees, the SCE of waterfront forests was most pronounced at 19:00, with air temperature reductions of 0.71–2.38°C in the four cases compared with the baseline scenario.

This study provides scientific insights for guidance in the planning and design of waterfront areas, which should be included in strategic urban planning policies. Notably, these UCI effects depended strongly on the waterfront land cover in the immediate environment of the

measurement sites; lawn was found to be thermally unsuitable for waterfront land-use. More research is needed to qualify the co-effect of green and blue spaces on UHI and air pollution and to estimate the spatiotemporal characteristics of thermal environment improvement by SCEs via a comprehensive comfort index.

Acknowledgments

This research work was supported by the National Key R&D Program of China (No. 2017YFC0702900).

References

- [1] Cheng, L., Guan, D., Zhou, L., Zhao, Z., & Zhou, J. (2019). Urban cooling island effect of the main river on a landscape scale in Chongqing, China. *Sustainable Cities and Society*, 47, 101501.
- [2] Shi, D., Gao, Y., Guo, R., Levinson, R., Sun, Z., & Li, B. (2018). Life cycle assessment of white roof and sedum-tray garden roof for office buildings in China. *Sustainable Cities and Society*, 40, 428–439.
- [3] Zhang, Y., Shi, D., Guo, R., Zhuang, C., Gao, Y., & Zhao, K. (2020). Single image modeling (SIM) for predicting the temperature and airflows of outdoor air zones in regional planning. *Sustainable Cities and Society*, 53, 101934.
- [4] Debbage, N., & Shepherd, J.M. (2015). The urban heat island effect and city contiguity. *Computers, Environment and Urban Systems*, 54, 181–194.
- [5] He, B. J. (2019). Towards the next generation of green building for urban heat island mitigation: zero UHI effect building. *Sustainable Cities & Society*, 101647. <https://doi.org/10.1016/j.scs.2019.101647>
- [6] Nesshöver, C., Assmuth, T., Irvine, K.N., Rusch, G.M., Waylen, K.A., Delbaere, B., Wittmer, H. (2017). The science, policy and practice of nature-based solutions: an interdisciplinary perspective. *Science of the Total Environment*, 579, 1215–1227.
- [7] Yan, H., Wu, F., & Dong, L. (2018). Influence of a large urban park on the local urban thermal environment. *Science of the Total Environment*, 622-623, 882–891.
- [8] Li, C., & Yu, C.W. (2014). Mitigation of urban heat development by cool island effect of green space and water body. Proceedings of the 8th International Symposium on Heating, Ventilation and Air Conditioning. Springer, 551–561.
- [9] Völker, S., Baumeister, H., Claßen, T., Hornberg, C., & Kistemann, T. (2013). Evidence for the temperature-mitigating capacity of urban blue space – a health geographic perspective. *Erdkunde*, 67,

355–371.

- [10] Cheng, L., Guan, D., Zhou, L., Zhao, Z., & Zhou, J. (2019). Urban cooling island effect of main river on a landscape scale in Chongqing, China. *Sustainable Cities and Society*, 47, 101501.
- [11] Ballinas, M., & Barradas, V.L. (2016). Transpiration and stomatal conductance as potential mechanisms to mitigate the heat load in Mexico City. *Urban Forestry & Urban Greening*, 20, 152–159.
- [12] Tan, Z., Lau, K.L., & Ng, E. (2015). Urban tree design approaches for mitigating daytime urban heat island effects in a high-density urban environment. *Energy and Buildings*, 114, 265–274.
- [13] Wu, C., Li, J., Wang, C., et al. (2019). Understanding the relationship between urban blue infrastructure and land surface temperature. *Sustainable Cities and Society*, 694, 133742.
- [14] Wang, Y., Ni, Z., Chen, S., & Xia, B. (2019). Microclimate regulation and energy-saving potential from different urban green infrastructures in a subtropical city. *Journal of Cleaner Production*, 226, 913–927.
- [15] Theeuwes, N.E., Solcerová, A., & Steeneveld, G.J. (2013). Modeling the influence of open water surfaces on the summertime temperature and thermal comfort in the city. *Journal of Geophysical Research: Atmospheres*, 118(16), 8881–8896.
- [16] Skelhorn, C., Lindley, S., & Levermore, G. (2014). The effect of vegetation types on air and surface temperatures in a temperate city: A fine scale assessment in Manchester, UK. *Landscape and Urban Planning*, 121, 129–140.
- [17] Wenze, Y., & Lihua, X. (2013). Thermal environmental effects of typical urban water landscape. *Acta Ecologica Sinica*, 33 (6), 1853–1859.
- [18] Anjos, M., & Lopes, A. (2017). Urban heat island and park cool island intensities in the coastal city of Aracaju, North-Eastern Brazil. *Sustainability*, 9, 1379.
- [19] Sun, R., Chen, A., Chen, L., & Lü, Y. (2012). Cooling effects of wetlands in an urban region: the case of Beijing. *Ecological Indicators*, 20, 57–64.
- [20] Nastran, M., Kobal, M., & Eler, K. (2019). Urban heat islands in relation to green land use in European cities. *Urban Forestry & Urban Greening*, 37, 33–41.
- [21] Wang, Y., & Akbari, H. (2016). The effects of forest planting on urban heat island mitigation in Montreal. *Sustainable Cities and Society*, 27, 122–128.
- [22] Hathway, E.A., & Sharples, S. (2012) The interaction of rivers and urban form in mitigating the urban heat island effect: a UK case study. *Building and Environment*, 58, 14–22.
- [23] Han, G., Chen, H., Yuan, L., Cai, Y., & Han, M. (2011). Field measurements on microclimate and

- cooling effect of river wind on urban blocks in Wuhan city. International Conference on Multimedia Technology (ICMT).
- [24] Steeneveld, G.J., Koopmans, S., Heusinkveld, B.G., & Theeuwes, N.E. (2014). Refreshing the role of open water surfaces on mitigating the maximum urban heat island effect. *Landscape and Urban Planning*, 121, 92–96.
- [25] Vahid, A.P., Esmail, S., Ahmad, R.Y., & van Bodegom, P.M. (2019). Analyzing temporal changes in urban forest structure and the effect on air quality improvement. *Sustainable Cities and Society*, 48, 101548.
- [26] Nowak, D.J. (1994) Air pollution removal by Chicago's urban forest. Chicago's urban forest ecosystem: results of the Chicago urban forest climate project.
- [27] Indra, J.C., & Dheeraj, R. (2019). Dust pollution: its removal and effect on foliage physiology of urban trees. *Sustainable Cities and Society*, 51, 101696.
- [28] Zhu, D., & Zhou, X. (2019). Effect of urban water bodies on distribution characteristics of particulate matters and NO₂. *Sustainable Cities and Society*, 50, 101679.
- [29] Lou, C., Liu, H., Li, Y., Peng, Y., Wang, J., & Dai, L. (2017). Relationships of relative humidity with PM_{2.5} and PM₁₀ in the Yangtze River Delta, China. *Environmental Monitoring and Assessment*, 189(11), 582.
- [30] Tang, T.R., Yuan, M.Q., & Cao, F. (2016). Characteristics analysis on distribution of particulate matters between lake shore cities and Taihu Lake. *Journal of the Meteorological Sciences*, 36, 819–825.
- [31] Zhang, Y., Zhan, Y., Yu, T., & Ren, X. (2017). Urban green effects on land surface temperature caused by surface characteristics: a case study of summer Beijing metropolitan region. *Infrared Physics and Technology*, 86, 35–43.
- [32] Dai, Z., Guldmann, J.M., & Hu, Y. (2018). Spatial regression models of park and land-use effects on the urban heat island in central Beijing. *Science of the Total Environment*, 626, 1136–1147.
- [33] Kellert, S.R., Heerwagen, J., & Mador, M. (2011). Biophilic design: the theory, science and practice of bringing buildings to life. John Wiley & Sons, Hoboken, New Jersey.
- [34] Xu, J., Wei, Q., Huang, X., Zhu, X., & Li, G. (2010). Evaluation of human thermal comfort near urban waterbody during summer. *Building and Environment*, 45, 1072–1080.
- [35] Pelorosso, R., Gobattoni, F., & Leone, A. (2017). Green courtyards as urban cool islands: towards nature-based climate adaptation plans of compact cities. *CSE-City Safety Energy*, 1, 27–36.
- [36] Du, H., Cai, Y., Zhou, F., Jiang, H., Jiang, W., & Xu, Y. (2019). Urban blue-green space planning

- based on thermal environment simulation: a case study of Shanghai, China. *Ecological Indicators*, 106, 105501.
- [37] The Chinese Weather Net, The Chongqing Climate Effect Assessment. Retrieved from <http://cq.weather.com.cn/qxfwcp/yqhpj/10/2206541.shtml>.
- [38] Gunawardena, K.R., Wells, M.J., & Kershaw, T. (2017). Utilising green and bluespace to mitigate urban heat island intensity. *Science of the Total Environment*, 584-585, 1040–1055.
- [39] Liu, Y.X., Fang, W., & Ma, L.H. (2013). Investigation on plant resources of Jungian branch in Chongqing and its vertical greening advantages. *Forestry Investigation and Planning*, 6, 124–128.
- [40] Gao, Y., Shi, D., Levinson, R., Guo, R., Lin, C., & Ge, J. (2017). Thermal performance and energy savings of white and sedum-tray garden roof: a case study in a Chongqing office building. *Energy and Building*, 156, 343–359.
- [41] ENVI-met [EB/OL]. Retrieved from <http://www.envi-met.com/>
- [42] Steele, M.K., & Heffernan, J.B. (2014). Morphological characteristics of urban water bodies: Mechanisms of change and implications for ecosystem function. *Ecological Applications*, 24, 1070–1084.
- [43] Toudert, F.A. (2005). Dependence of outdoor thermal comfort on forest design in hot and day climate (Doctoral dissertation, Berichte des Meteorologischen Institutes der Universität Freiburg).
- [44] Samaali, M., Courault, D., Bruse, M., et al. (2007). Analysis of 3D boundary layer model at local scale validation on soybean surface radiative measurements. *Atmospheric Research*, 85, 183–198.
- [45] Quah, A.K.L., & Roth, M. (2012). Diurnal and weekly variation of anthropogenic heat emissions in a tropical city, Singapore. *Atmospheric Environment*, 46(1), 92–103.
- [46] Huttner, S. (2012). Further development and application of the 3D microclimate simulation ENVI-met. Mainz: Johannes Gutenberg-Universität in Mainz.
- [47] Chow, W.T.L., & Brazel, A.J. (2012). Assessing xeriscaping as a sustainable heat island mitigation approach for a desert city. *Building and Environment*, 47, 170–181.
- [48] Ministry of Construction, China. (2016). Code for thermal design of civil buildings (GB50176-2016). China Planning Press.
- [49] Ministry of Housing and Urban-Rural Development, China. (2013). Design standards for thermal environment of urban residential areas (JGJ286-2013). China Planning Press.
- [50] Zheng, M., Fang, W., Ma, L., An, S., Wang, H., & Xing, Y. (2017). Atmospheric particle retaining function of common tree species leaves in urban areas of Chongqing. *Forest Inventory and Planning*, 42, 25–31. doi:10.3969/j.issn.1671-3168.2017.01.006.

- [51] Chow, W.T.L., Pope R.L., Martin C.A., et al. (2010). Observing and modeling the nocturnal park cool island of an arid city: horizontal and vertical effects. *Theoretical & Applied Climatology*, 103(1–2), 197–211.
- [52] Yang, X. (2012). Outdoor microclimate simulation study of the effect of building energy consumption of air conditioning. (Doctoral dissertation, South China University of Technology).
- [53] Tsoka, S., Tsikaloudaki, A., & Theodosiou, T. (2018). Analyzing the ENVI-met microclimate model's performance and assessing cool materials and urban vegetation applications – a review. *Sustainable Cities and Society*, 43, 55–76.
- [54] Zhao, Q., Sailor, D.J., & Wentz, E.A. (2018). Effect of tree locations and arrangements on outdoor microclimates and human thermal comfort in an urban residential environment. *Urban Forestry & Urban Greening*, S1618866717305666.
- [55] Zhang, L., Zhan, Q., & Lan, Y. (2018). Effects of the tree distribution and species on outdoor environment conditions in a hot summer and cold winter zone: a case study in Wuhan residential quarters. *Building and Environment*, 130, 27–39.
- [56] Yanyan, H., Xiang, C., & He Q. (2017). Distribution characteristics and evaluation of heavy metals in soil of urban expressway greenbelt in main urban area of Chongqing. *Landscape science and technology* (4), 12-14.
- [57] Song, J., Wang, Z.-H., & Wang, C. (2018). The regional effect of urban heat mitigation strategies on planetary boundary layer dynamics over a semiarid city. *Journal of Geophysical Research: Atmospheres*, 123. <https://doi.org/10.1029/2018JD028302>.
- [58] Heisler, G.M., & Grant, R.H. (2000). Ultraviolet radiation in urban ecosystems with consideration of effects on human health. *Urban Ecosystems*, 4(3), 193–229.
- [59] Yang, F., Lau, S.S.Y., & Qian, F. (2011). Urban design to lower summertime outdoor temperatures: An empirical study on high-rise housing in Shanghai. *Building and Environment*, 46(3), 769–785.
- [60] Wang, Y., Bakker, F., de Groot, R., & Wörtche, H. (2014). Effect of ecosystem services provided by urban green infrastructure on indoor environment: A literature review. *Building and Environment*, 77, 88–100.
- [61] Shuko, H., & Takeshi, O. (2010). Seasonal variations in the cooling effect of urban green areas on surrounding urban areas. *Urban Forestry & Urban Greening*, 9, 15–24.
- [62] Jauregui, E. (1991). Influence of a large urban park on temperature and convective precipitation in a tropical city. *Energy and Buildings*, 15(3), 457–463.
- [63] Syafii, N.I., Ichinose, M., Kumakura, K., Jusuf, S.K., Chigusa, K., & Wong, N.H. (2017). Thermal

environment assessment around bodies of water in urban canyons: A scale model study. *Sustainable Cities and Society*, 34, 79–89.

[64] Hayden, K.L., Sills, D.M.L., Brook, J.R., Li, S.M., Makar, P.A., Markovic, M.Z., et al. (2011). Aircraft study of the effect of lake-breeze circulations on trace gases and particles during BAQS-Met 2007. *Atmospheric Chemistry and Physics*, 11, 10173–10192.

[65] Martins, T.A.L., Adolphe, L., Bonhomme, M., Bonneaud, F., Faraut, S., Ginestet, S., Michel, C., & Guyard, W. (2016). Effect of urban cool island measures on outdoor climate and pedestrian comfort: Simulations for a new district of Toulouse, France. *Sustainable Cities and Society*, 26, 9–26.